Fretting Wear and Lubrication Characteristics of the Steel Ring of a Metal Belt-Type Continuously Variable Transmission

Ling Han (hanling@ccut.edu.cn)
Changchun University of Technology
Wei Zhao
Changchun University of Technology
Yue Cao
Changchun University of Technology
Wu Jin Wang
Changchun University of Technology

Research Article

Keywords: Continuously variable speed , Fretting wear , Fretting frequency , Lubrication characteristics , Safety margin

Posted Date: March 22nd, 2022

DOI: https://doi.org/10.21203/rs.3.rs-1234072/v1

Title page

Fretting Wear and Lubrication Characteristics of the Steel Ring of a Metal Belt-Type Continuously Variable Transmission

Ling Han, born in 1984, is an associate professor at *Changchun University of Technology*. He graduated from *Jilin University* with a doctorate degree. The research direction is transmission theory and transmission mechanism control research.
Tel: 13578997844; Email: hanling@ccut.edu.cn

Wei Zhao, born in 1997, is a postgraduate of *Changchun University of Technology*. The research direction is the research of transmission theory and control of transmission mechanism.
Email: zw656488556@126.com

Yue Cao, is a postgraduate tutor at *Changchun University of Technology*. The research direction is the research of transmission theory and control of transmission mechanism.
E-mail:caoyue@ccut.edu.cn

Jin-Wu Wang, is a postgraduate tutor at *Changchun University of Technology*. The research direction is the research of transmission theory and control of transmission mechanism.
*E-mail: wangjinwu@ccut.edu.cn

Corresponding author：Jin-Wu Wang * E-mail：wangjinwu@ccut.edu.cn

Fretting Wear and Lubrication Characteristics of the Steel Ring of a Metal Belt-Type Continuously Variable Transmission

Ling Han，Wei Zhao，Yue Cao，Jinwu Wang*

Received June xx, 201x; revised February xx, 201x; accepted March xx, 201x

Abstract: The multi-field coupling mechanism of a continuously variable transmission (CVT) system has a greater impact on its overall friction loss. The friction loss of steel rings represents the internal loss of the metal belt occurring between the steel ring group and friction plate, and it is the main reason for the loss of CVT energy. This study is based on the dissipative wear model of the CVT steel ring friction pair, and it innovatively establishes a steel ring wear depth model that relates the wear depth to the macro- and micro-factors. Here, a mixed lubrication model between the friction pairs of steel rings is constructed, and the change law of oil film thickness, pressure, and temperature between the contacting bodies is obtained. On the basis of the wear depth model of the steel ring, the results of the wear depth of the steel ring are obtained via simulation using torque, speed, fretting frequency, and other operating parameters. The surface wear of the steel ring at different fretting frequencies is observed via SEM, and the simulation and test results are compared. Subsequently, the obtained results of the wear depth and oil film thickness tests are used to determine the safety margin of the application efficiency of the steel ring friction pair in the CVT working range via the interpolation processing method. According to the simulation results, the overall performance area of the safety margin of the application efficiency of the steel ring friction pair is between −1 and 1. When the torque is greater than 130 N•m, the safety margin value decreases below 0, the safety failure probability of the steel ring increases significantly, and the safety margin decreases gradually. This research can provide new insights into solving the reliability and service life of CVTs.
Keywords: Continuously variable speed • Fretting wear • Fretting frequency • Lubrication characteristics • Safety margin

1 Introduction

The metal belt-type continuously variable transmission (CVT), which is the core component of automobile transmission devices, allows the transmission power to function continuously at the optimal operating point; thus, it has been widely used in various types of automobiles [1-3]. However, transmission conditions of CVTs are complex and changeable, and the loss generated at this period cannot be ignored because it directly affects the transmission efficiency of the CVT and its service life [4-5]. The thermal–mechanical–hydraulic multi-field coupling of the CVT steel ring should also be considered because the contact characteristics and lubrication state of each steel ring layer under the relative movement of the friction plate gradually forms a surface damage with the regular distribution of stress, strain, and temperature [6-7]. Furthermore, as the load changes, fretting slippage and wear occur between the mating surfaces of the steel ring [8-9]. The transmission through the friction plate will alter the contact characteristics and relative movement between the belt and pulley, further resulting in metal belt slippage, pulley deflection, and bearing creep while simultaneously generating noise [10-11]. Therefore, the effect of the micro-motion phenomenon of the steel ring and the lubrication state between the mating surfaces on the overall application efficiency of the transmission must be fully understood. The influence of service life under the multi-field coupling should also be determined.

In recent years, the research on the improvement of automotive application efficiency has become increasingly mature, but the impact of micro-motion frequency and macro-parameters on the application efficiency and service life of mechanical systems is rarely investigated. Some scholars have studied the fretting corrosion effect of the 690TT alloy tube and 405 stainless steel plate under high temperature and high pressure water [12-13] and found that the wear volume of the 690TT tube first increases and then decreases with the increase in fretting frequency. As the wear volume of the 405 stainless steel plate accumulates, life prediction models have been proposed accordingly. The type of debris also has a certain effect on fretting wear [14-15]. Kirk et al. [16-17] offered new insights into the frequency effects by studying the influence of displacement amplitude on fretting wear within a frequency range. Their findings indicate that the increase in vibration frequency will alter the oxidation-based wear mechanism into one that cannot form an oxidized debris layer. Furthermore, the oxidized debris will isolate the direct contact of the contact surface and cause serious underground damage. Xin et al. [18-19] investigated the influence of frequency on the fretting corrosion behavior of the type 304 stainless steel and its mechanism under high temperature and high pressure water. Their results showed that the main sources of wear are delamination wear, material transfer wear, and oxidative wear. The increase in frequency accelerates the escape of wear debris, which is not only caused by the damage of the TTS layer but also by the fragmentation of oxidized particles between the contact surfaces. The effect of temperature on fretting wear cannot be ignored. Temperature not only will affect the change in geometric shape of the friction pair but also the contact characteristics between the friction surfaces [20-22]. Srivastava et al. [23] proposed a finite element-based fretting and fretting fatigue prediction method for compression shafts. This method combines the wear model with fretting fatigue analysis to quantitatively predict the effect of stress redistribution caused by fretting wear. Their results showed that

[1]✉Jin-Wu Wang
Wangjinwu@ccut.edu.cn

[1] Changchun University of Technology, Changchun 130,000, China

the contact edge stress is the most significant parameter. Fu Bing et al. [24] focused on the problem of low transmission efficiency of an existing CVT, constructed a steel ring friction loss calculation model by deriving the corresponding steel ring pressure model and steel ring kinematics model, and analyzed the torque, speed, and speed ratio. The steel ring and its influence on friction loss were explored, and the findings were verified through bench tests. Their metal belt structure was improved by implementing an optimization design for transmission efficiency. In summary, the input torque and rotating speed of CVTs and the fretting frequency of steel rings greatly affect fretting wear. Consequently, the relationships of the aforementioned aspects should be explored to improve the application efficiency and service life of CVTs.

The lubrication state of mechanical systems and the corresponding service life has aroused widespread attention in the scientific research field, and scholars have increasingly studied the characteristics of lubricating oil films [25-27]. Wang [28-29] comprehensively studied the lubrication-dynamic contact oil film stiffness of point-contact spiral bevel gears under periodically fluctuating loads and speeds and found a competitive relationship between dynamic load and contact area. Positive or negative stiffness flipping, which caused either extremely low or high stiffness, were observed at certain fluctuation amplitudes. Wang [30], using the crowned double-helical gears in point-contact hybrid elastohydrodynamic lubrication (EHL), extended Archard theory to the lubrication situation. The wear rate of the point-contact hybrid EHL was evaluated, and the effect of surface roughness on wear life was obtained. A wear life prediction model was proposed to improve the wear life of the crown double-helical gears by reasonably matching the lubrication, dressing, and working parameters. Other scholars have studied the influence of torque, speed, roughness, and other factors on the transient mixed lubrication state of friction pair surfaces to explore their internal relationship. By optimizing and improving the existing methods, the stability and service life of mechanical systems can be improved [31-33]. Chun et al. [34-35] proposed a thermal hybrid lubrication model to investigate the effect of temperature on the mechanical properties and tribological properties of coating. In summary, scholars have applied many methods to study the lubrication characteristics of different mechanical systems. Here, the CVT steel ring is taken as the research object, and the film thickness, pressure, and temperature distribution of the lubricating oil film are simulated under specific working conditions. The results can lay the foundation for comprehensively understanding the safety margin of the friction pair of steel rings.

In particular, this study explores the influence of CVT input torque, speed, and fretting frequency on the wear depth of the steel ring friction pair. By means of modeling and simulation, the lubrication relationship between the two friction pairs is explored, and the random oil film distribution between them is obtained. Moreover, the changes in lubricating oil film thickness, pressure, and temperature are determined. The rough morphology and wear state of the surface of the friction pair are observed via SEM, and the influence of the different fretting frequencies is analyzed. Finally, the CVT safety margin related to the wear depth and the oil film thickness is obtained.

2 Theory

The CVT metal belt is composed of hundreds of metal friction plates and 6 to 12 layers of steel rings. The transmission and structure diagrams are shown in the figure. The steel ring group is tensioned under the action of clamping force of the metal pulley to prop up the friction plate for torque transmission. When the CVT is in service, the relative sliding and vibration between the steel ring and another steel ring, between the steel ring and saddle surface of the friction lining, and other factors cause a wear between the steel rings. As the loss of the first-layer steel ring accounts for 70% of the total friction power loss of the steel ring, the loss of the second to ninth layer of steel ring is only 6% to 0.008% [24]. Thus, the loss ratio of the first-layer steel ring is much greater than that of other steel rings. The research object of this study comprises the first- and second-layer steel rings. The observation diagram of the surface wear of these steel rings and the diagram of the CVT and structure are shown in Figs. 1 and 2, respectively.

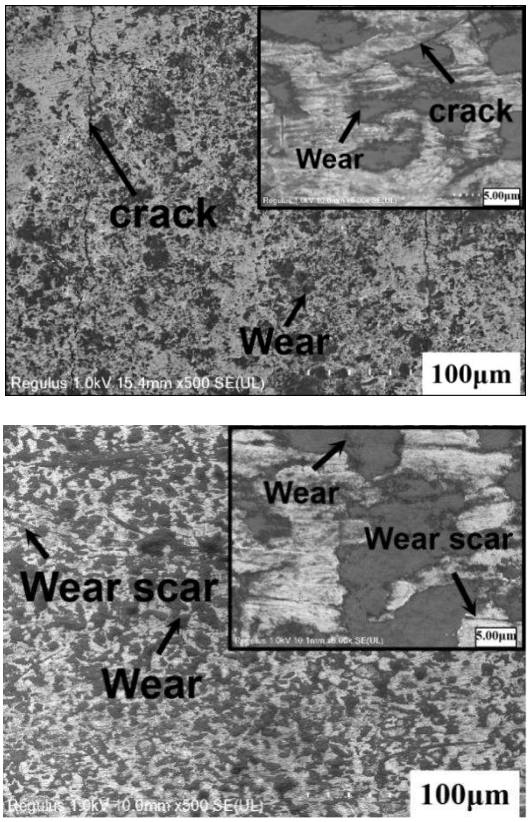

Fig. 1. Observation diagram of the surface wear of steel ring

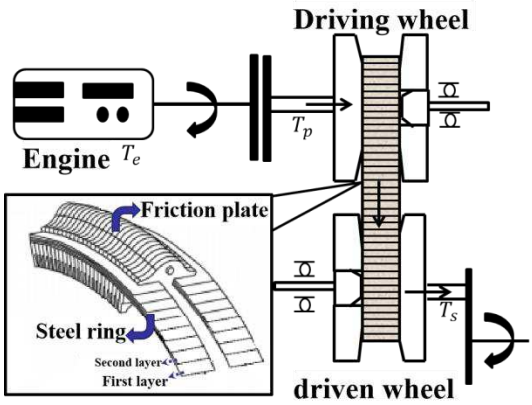

Fig. 2 Continuously variable transmission transmission and structure diagram

2.1 Wear modeling

Many models can be used to calculate wear and tear, and the scope of their adaptation varies. At present, the most widely used wear model in engineering is the Archard-related adhesive wear model [36].

$$V = k\frac{PS}{H} \tag{1}$$

where k is the wear coefficient; P is the contact normal load; S is the sliding distance; and H is the material hardness.

When the Archard model calculates wear, it can only be applied when the friction factor is constant. Taking into account the complexity and variability of the surface material wear process of the friction pair of the CVT steel ring, friction and wear modeling under variable load conditions is required [37,38]. On the basis of the corresponding energy point, the aforementioned process can be regarded as the result of energy consumption and conversion. Moreover, the friction pair produces a material surface wear due to the energy consumption during the friction process.

Dissipation theory [39] assumes a linear relationship between the amount of fretting wear and the dissipated energy as follows:

$$V = \upsilon\sum_{i=1}^{k} Ed_i \tag{2}$$

where υ is the energy wear coefficient; Ed_i is the energy dissipation of a single micro-motion cycle under a given slip amplitude; and K is the number of wear cycles.

Dissipated energy, which is the friction work related to shear force, is expressed as

$$Ed_i = \int F_{Si}ds_i \tag{3}$$

where F_{s_i} is the total force of the i fretting friction metal belt, and S_i is the relative sliding distance of the two steel ring friction pairs with i fretting friction.

In the research process, the contact area is set as the limit contact area dA, and the fretting wear depth dh is given by

$$dh = \frac{dV}{dA} = \upsilon_s\sum_{i=1}^{k}\left(dE_{d_i}/dA\right) \tag{4}$$

where is the local wear coefficient.

According to Eq. (3), the i local wear dissipation energy dE_{d_i} at any X of the steel ring arc can be obtained as follows:

$$dE_{d_i} = F_{S_i}(x)ds_i(x) \tag{5}$$

where $F_{s_i}(x)$ is the total force at the local position of the first- and second-layer steel rings of the i fretting friction, and $ds_i(x)$ is the relative sliding of the local position X for the move distance of the first- and second-layer steel rings of the i fretting friction.

From Eqs. (4) and (5), the wear depth of the contact position of the first- and second-layer steel rings of the i fretting friction can be expressed as follows:

$$dh = \upsilon_S\sum_{i=1}^{k}\tau_i(x)ds_i(x) \tag{6}$$

where $\tau_i(x)$ is the friction shear stress at the local contact position X of the first- and second-layer steel rings of the i fretting friction.

Subsequently, the fretting depth can be obtained as follows:

$$\Delta h_i(x) = \upsilon_s\int\tau_i(x)ds_i(x) \tag{7}$$

Assuming K_{int} incremental steps in the continuous fretting friction process, the wear depth denoted by $j(j = 1,2\cdots, K_{\mathrm{int}})$ can be linearly superimposed to obtain the local contact position of the first- and second-layer steel rings of the i fretting friction. Thus,

$$\Delta h_i(x) = \upsilon_s\sum_{j=1}^{K_{int}}\tau_{i,j}(x)ds_{i,j}(x) \tag{8}$$

where $\tau_{i,j}(x)$ is the shear stress of the j wear increment under i fretting friction, and $ds_{i,j}(x)$ is the relative slip distance of the j wear increment under i fretting friction.

The wear depth at the local contact position of the steel ring under K fretting friction can be expressed as

$$h(x) = \upsilon_s\sum_{i=1}^{K}\sum_{j=1}^{K_{int}}\tau_{i,j}(x)ds_{i,j}(x) \tag{9}$$

In the actual fretting friction process, the number of frictions is quite large. Sequentially measuring the friction in the calculation process will increase the operation and time cost. However, as the amount of wear caused by each fretting friction is extremely small, the succeeding wear result will only be slightly affected. Therefore, the energy wear coefficient can be appropriately increased through the principle of similarity. At the same time, the fretting friction process can be substituted for ΔK friction processes, consequently greatly shortening the calculation time.

Let the number of accelerations be ΔK. The wear depth at the local position X of the steel ring during the entire fretting friction process can be expressed as

$$h(x) = \Delta K\sum_{i=1}^{K/\Delta K}\sum_{j=1}^{K_{int}}\upsilon_s\tau_{i,j}(x)ds_{i,j}(x) \tag{10}$$

The metal surface in contact with air has a surface film that is naturally polluted. To resolve potential friction and sliding issues, the film needs to be cut.

Let the shear strength of the film be $\tau_{i,j}(x)$. If the metal shear strength τ_b is used as the unit to express $\tau_{i,j}(x)$, then it can be written as $\tau_{i,j}(x) = C\tau_b$, where C is a constant.

$$f = \frac{C\tau_b}{\sigma_s} = \frac{\tau_{i,j}(x)}{\sigma_s} \tag{11}$$

Eq. (11) summarizes the universality of various surface states, including adhesion friction and the friction of oxide film and other reactive films.

The clamping force exerted on the steel ring in Eq. (11) can be expressed as

$$F_{S_i} = \frac{S_f T_p\cos\alpha}{2fR_p} \tag{12}$$

where S_f is the safety factor; T_p is the input torque of the driven wheel; α is the cone angle of the pulley; f is the friction factor; and R_p is the working radius of the driving wheel.

The change in operating conditions during the transmission process of CVTs is variable and entails multi-excitation characteristics. Thus, the transmission load at this time is also changed. Assuming that the transmission load can be changed in

the form of simple harmonics, then the torque transmitted by the steel ring friction pair can be expressed as follows:

$$T_t = k_v T_m \left[1 + \varepsilon \cos\left(\omega t + \varsigma\right)\right] \tag{13}$$

where k_v is the dynamic load coefficient related to speed; T_m is the average input torque; ε is the input torque amplitude fluctuation coefficient; ω is the fretting frequency; ς is the difference between the common tangent of the working circle of the master and driven wheel and connecting center line and the angle between them.

On the basis of Eq. (13), the shear stress can be obtained as follows:

$$\tau_{i,j}(x) = \frac{2F_{si}R_p}{S_f k_v T_m \sigma_s \left[1 + \varepsilon \cos\left(\omega t + \varsigma\right)\right] \cos\alpha} \tag{14}$$

$$h(x) = \Delta K \sum_{i=1}^{K/\Delta K} \sum_{j=1}^{K_{int}} \upsilon_s \frac{2F_{si}R_p}{S_f k_v T_m \sigma_s \left[1 + \varepsilon \cos\left(\omega t + \varsigma\right)\right] \cos\alpha} ds_{i,j}(x) \tag{15}$$

2.2 Lubrication model

The metal belt transmits torque through thrust and friction, and the lubrication between the friction pairs conforms with the form of the thermal elastohydrodynamic point contact. In this regard, the Reynolds equation is considered. The Reynolds equation is given by

$$\frac{\partial}{\partial x}\left(\frac{\rho h^3}{\eta}\frac{\partial p}{\partial x}\right) + \frac{\partial}{\partial y}\left(\frac{\rho h^3}{\eta}\frac{\partial p}{\partial y}\right) = 6u_s\rho\frac{\partial h}{\partial x} + 6u_s h\frac{\partial p}{\partial x} \tag{16}$$

where X and Y are the directions of the coordinate system; h is the thickness of the oil film; and ρ and η represent the influence of temperature on the density and viscosity of the lubricating oil, which can be obtained using the density, temperature, and pressure equation and the viscosity, temperature, and pressure equation [40].

When the outlet and inlet zone pressures are both 0 and the outlet zone pressure change rate is 0, the boundary conditions of the equation are as follows:

Entrance: $p(x_1, y) = 0$ and

Exit: $p(x_2, y) = 0$, $\frac{\partial p(x_2 y)}{\partial x} = 0$,

where x_1 is the X coordinate at the entrance, and x_2 is the X coordinate at the exit.

The point-contact film thickness equation that considers roughness can be expressed as follows:

$$h_1 = h_0 + \frac{x^2}{2R_x} + \frac{y^2}{2R_y} + h(x, y) + r(x, y) \tag{17}$$

$$h(x, y) = \frac{2}{\pi E}\iint_{\Omega}\frac{p(s,t)}{\sqrt{(x-s)^2 + (y-t)^2}}dsdt \tag{18}$$

$$E = \frac{1}{2}\left(\frac{1-\upsilon_1^2}{E_1} + \frac{1-\upsilon_2^2}{E_2}\right) \tag{19}$$

where h_0 is the central film thickness; R_x and R_y are the equivalent radius of curvature along the X, Y directions, respectively; $h(x, y)$ is the elastic deformation displacement caused by pressure; $r(x, y)$ is the surface roughness function; E is the comprehensive elastic modulus; S and g are the coordinates of the pressure point along the X and Y directions, respectively; E_1 and υ_1 represent the elastic modulus and Poisson's ratio of the metal sheet, respectively, and E_2 and υ_2 represent the elastic modulus and Poisson's ratio of the pulley, respectively.

The rough peaks between the steel rings are randomly distributed on the basis of the probability density function. Therefore, the number of contact peaks between them should also be calculated. The root mean-square values of surface roughness of the two friction pairs are denoted by σ_1 and σ_2, respectively. The contact between the steel rings can be converted into a contact between a smooth rigid surface and a rough elastic surface. The root mean-square value of the rough elastic surface is given by $\sigma = \sqrt{\sigma_1^2 + \sigma_2^2}$.

When the distance between the center lines of the rubbing pairs is 1 and when the profile height Z is greater than the center line distance 1, the surface of the steel ring will be in contact. In the probability density distribution curve, the area where two surfaces are in contact is the surface contact probability, which is given by

$$P(z > x) = \int_1^{\infty}\psi(z)dz \tag{20}$$

If the number of peak points of the rough surface is n, then the number of peak points of the contact part m can be expressed as

$$m = n\int_1^{\infty}\psi(z)dz \tag{21}$$

The normal deformation of the contact peak point is given by $z - 1$. The actual contact area A is expressed as

$$A = m\pi R\int_1^{\infty}(z-1) = n\pi R(z-1)\psi(z)dz \tag{22}$$

The total load W supported by the contact peak point is given by

$$W = \frac{4}{3}mER^{1/2}(z-1)^{3/2} = \frac{4}{3}nER^{1/2}\int_1^{\infty}(z-1)^{3/2}\psi(z)dz \tag{23}$$

Usually, the contour height of the actual surface is distributed according to Gauss. In Gauss distribution, the part near the larger Z value can be used to approximate the exponential distribution. Let $\psi(z) = \exp(-z/\sigma)$. Thus,

$$\left.\begin{aligned} m &= n\,exp(-1/\sigma) \\ A &= \pi nR\sigma\,exp(-1/\sigma) \\ W &= \frac{4}{3}nER^{1/2}\sigma^{3/2}\,exp(-1/\sigma) \end{aligned}\right\} r(x, y) \tag{24}$$

The heat transfer mode of the lubricating oil film is mainly convective heat dissipation. Furthermore, the heat transfer along the film thickness direction is negligible. The required energy equation can be expressed as

$$\left(\frac{u_s}{2}-\frac{h^3}{12\eta}\frac{\partial p}{\partial x}\right)\frac{\partial T}{\partial x}-\left(\frac{h^3}{12\eta}\frac{\partial p}{\partial y}\right)\frac{\partial T}{\partial y}= \frac{\eta u_s^2}{Jpc_p h}+\frac{h^3}{12\eta Jpc_p}\left[\left(\frac{\partial p}{\partial x}\right)^2+\left(\frac{\partial p}{\partial y}\right)^2\right] \tag{25}$$

where C_p is the equal-pressure specific heat capacity of the lubricating oil; T is the lubricating oil temperature; and J is the thermal power equivalent.

The degree of solution is from the inlet to the outlet along the direction of the oil film movement. Here, the X direction is set as the lubricating oil flow direction, T_0 is the dimensionless initial temperature. The boundary conditions are set as follows:

Along the X direction: $T(x_1, y) = T_0$;

Along the X direction: $\left.\frac{\partial T}{\partial y}\right|_{z=0} = 0$.

2.3 Finite element model

The CVT selected in this study is a nine-layer steel ring. Conceptually, the CVT separates the first-layer steel ring from the second-layer steel ring, and it facilitates the meshing and simulation of subsequent finite element calculations. ANSYS is used for the simulation calculation. In view of ensuring the accuracy of the calculation process, the minimum mesh length is set to 1 mm using the MultiZone method, and the element size is limited to 1 mm. The surface microstructure of the first- and second-layer steel rings are shown in Figs. 3(a) and (b), respectively. Fig. 3(c) shows the contact form of the friction pair. The friction pair is composed of two martensitic steel rings with a length of 20.0 mm and a thickness of 0.18 mm.

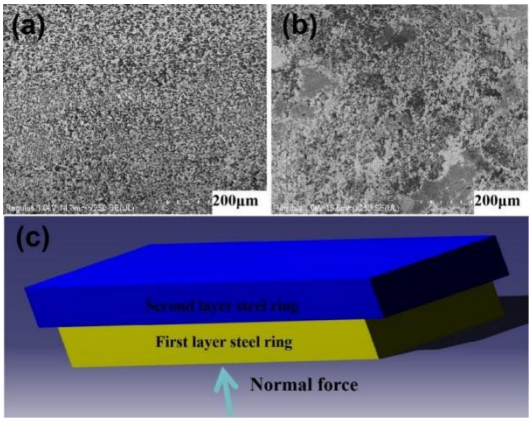

Fig. 3. The structure and contact model of the steel ring. (a) The surface morphology of the first layer of steel ring. (b) The surface morphology of the second layer of steel ring. (c) Contact form diagram of steel ring friction pair.

After setting the boundary conditions by using the established model, the temperature distribution of the steel ring as a whole under 3000 cycles is obtained via numerical methods. Fig. 4 shows the temperature distribution results. The rise in temperature is mainly concentrated in the area near the contact surface between the friction plate and the steel ring. When the CVT is in service, the internal measurement of the friction plate comes in contact with the steel ring side and produces relative sliding. The friction work causes the temperature to be relatively high with an obvious change. In addition, the saddle surface and the contact surface of the steel ring have a lubricating oil in between them. The heat dissipation between the saddle surface and the steel ring usually manifests in the form of heat dissipation that causes the temperature to be transmitted to the edge of the steel ring. In this case, the decrease is relatively fast, and the temperature rises but is not obvious.

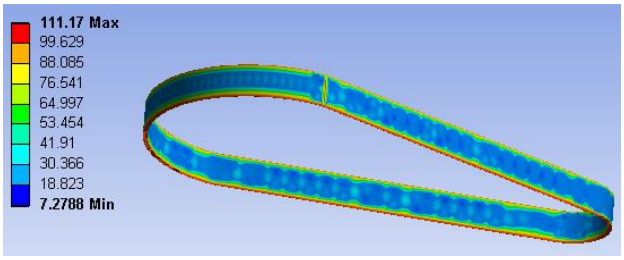

Fig. 4. Simulation diagram of the steel ring structure temperature

3 Results

3.1 Determine the cycle time

By taking the CVT as the research object, the relationship of fretting wear and fretting parameters between the first- and second-layer steel rings is calculated according to the abovementioned model. Prior to performing a simulation analysis of the interference section of the steel ring, the frequency of the micro-motion cycle K should be initially determined.

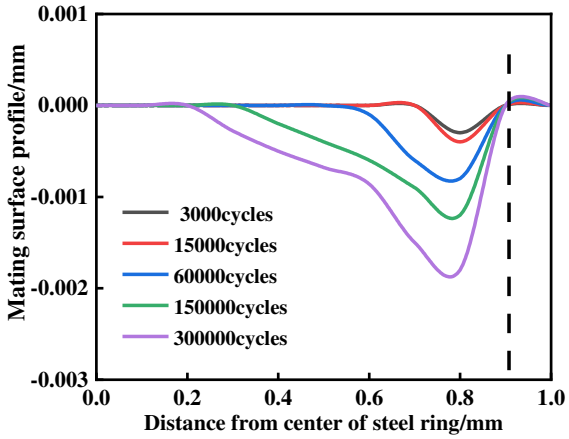

Fig. 5 Simulation results of steel ring mating surface profile

Fig. 5 shows the simulation results of the mating surface profile of the steel ring at different cycles. The abscissa represents the distance between any position of the steel ring and the center of the steel ring. Here, as the contour of the mating surface of the steel ring has the most apparent change at the edge of the plot, the contour within the range of 0–1.0 mm from the center of the steel ring is selected. The position at 0.9 mm represents the edge of the interference fit, while the left side represents the location of the interference fit. Fig. 6 shows that, in the same cycle, when the wear depth of the mating surface reaches the maximum at the extreme edge of the interference fit, it gradually decreases towards the center line of the steel ring. With the continuous increase in cycle time, the wear depth of the edge of the steel ring towards the centerline constantly increases, and the wear width also increases. In view of ensuring the accuracy of the results, as the roughness amplitude between the first- and second-layer steel rings is maintained close to 1 and the oscillation amplitude does not exceed 1, the smallest cycle of 3000 is selected in this study. In this manner, the degree of accuracy the contour wear of the mating surface can be guaranteed.

3.2 Influence of torque

Different T_m input torque values are selected for the simulation to explore the wear depth between the first- and second-layer steel rings by the transmitted torque. Fig. 6 shows the changes in wear depth of the steel ring surface along the axial direction of the transmission after the load cycle of the two friction pairs is set to 30, 90, and 150 N•m. Fig. 6(a) shows the wear depth distribution on the outer side of the first-layer steel ring friction pair. The wear depth from the inner side of the steel ring $(X/L=0)$ to the outer side $(X/L=1)$ decreases first and then increases. Then, the wear depth increases rapidly at $X/L=0.83$ and reaches the maximum at $X/L=1.0$. When the torque is $T_m=150N•m$, the maximum wear depth is 1.54 μm. Fig.6 (b) shows the distribution of the inner wear depth of the first-layer steel ring friction pair. The change trend is roughly the same as that of the tight edge of the steel ring, but the change trend is slower. Fig. 6(c) shows the wear depth distribution of the outer side of the second-layer steel ring friction pair. From the inner side of the steel ring $(X/L=0)$ to the outer side $(X/L=1)$, the wear depth first decreases and then increases. The wear depth increases rapidly at $X/L=0.86$ and reaches the maximum at $X/L=1.0$. At $T_m=150N•m$, the maximum wear depth is 3.1 μm. This finding can be attributed to the metal sheet that transmits the torque through the thrust force at the interference of the friction pair. Furthermore, the pressure on the steel ring increases, which causes the contact pressure and shear force of the fretting surface to increase, further causing the wear depth in this area to increase. Due to the pressure accumulation, the contact pressure and shear force manifest a stress concentration, and the wear depth of the interference area increases sharply.

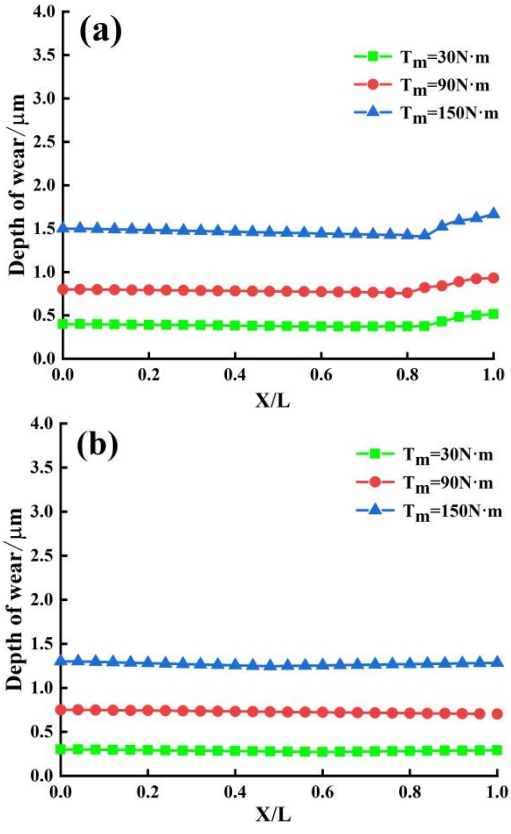

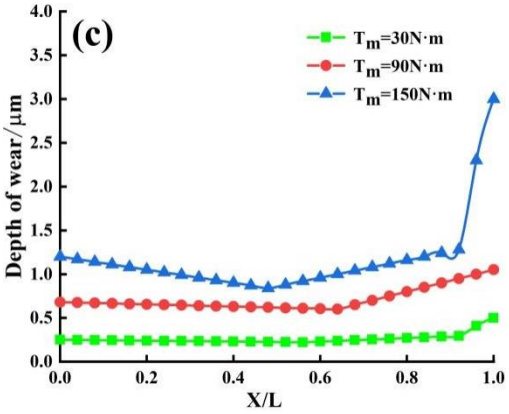

Fig. 6. Wear depths at different positions of the steel ring under varying torques: (a) outer side of the first-layer steel ring friction pair; (b) first-layer steel ring friction pair; and (c) outer side of the second-layer steel ring friction pair.

3.3 Influence of speed

Transmission speed is an important factor affecting the wear depth of steel rings. Here, the speed input values are set to 1400, 2100, and 2800 $r/\min$ to avoid reaching the maximum or minimum speed of the transmission during simulation. Fig. 7 shows the variation in wear depth of the friction pair at the tight, loose, and interference parts of the steel ring with the input speed. As shown in Fig.7 (a), the wear depth of the steel ring along the axial direction decreases first and then increases. The greater the speed, the greater the wear depth. The wear depth increases rapidly at $X/L=0.9$ because this area corresponds to the wear edge. The squeezing force of the transmission metal sheet on the steel ring is relatively large, resulting in a change in wear depth. As for the loose edge of the steel ring, its change in wear depth is similar to that of the tight edge; however, as the pushing force onto the steel ring by the metal sheet is smaller than that of the tight edge, the wear depth and the corresponding amplitude change are smaller. Fig. 7(c) shows the change in wear depth of the outer side of the second-layer steel ring. The change trend first decreases and then rapidly increases at approximately $X/L=0.5$, and the increase is even faster at approximately $X/L=0.9$. This trend can be attributed to the two positions where the metal sheet enters and leaves the metal pulley. Owing to the pushing force of the metal sheet, the steel ring entrains the metal sheet to move together, and a relative position is achieved when entering and leaving the metal pulley. Given the relatively high pressure in this area, the wear frequency is relatively fast, resulting in a much faster increase in the wear depth of the steel ring.

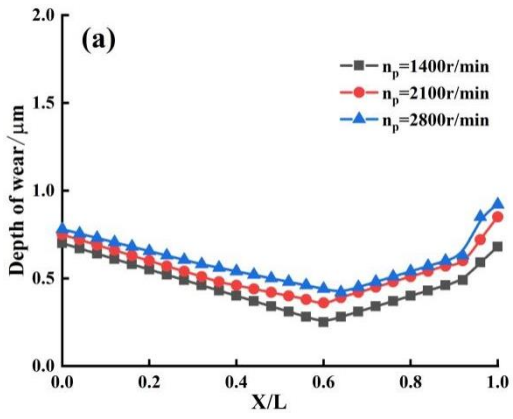

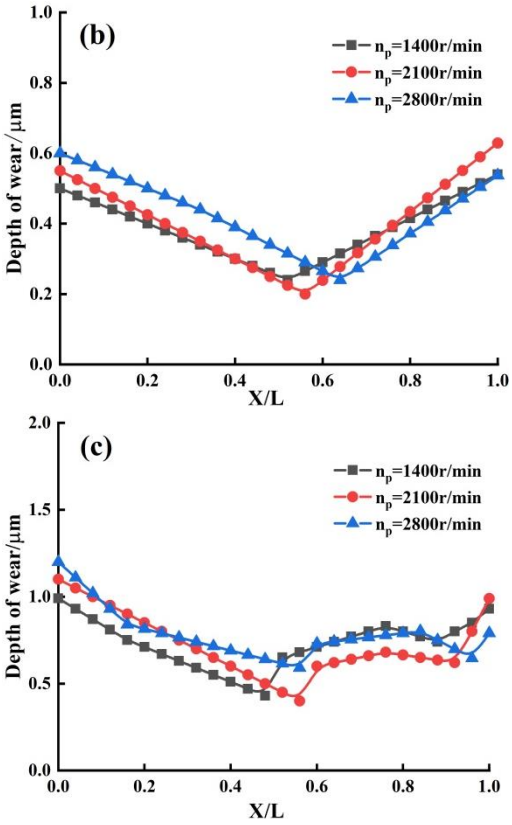

Fig. 7. Wear depths at different positions of the steel ring under varying speeds: (a) outer side of the first-layer steel ring friction pair; (b) first-layer steel ring friction pair; and (c) outer side of the second-layer steel ring friction pair.

3.4 Influence of fretting frequency

The material of the transmission steel ring friction pair used in this study is a maraging rigidity with a yield limit of 175 of 18% Ni, and various age-hardening alloy elements are added to its composition. Table 1 shows the chemical composition of the martensitic steel ring. The elastic modulus is 192 GPa, the Poisson's ratio is 0.30, and the density is 7800 kg/m^3. The specimens are cleaned in ethanol and processed in a dryer prior to the test.

Table 1 Maraging rigid composition table

Sample	Ingredients
Ni	17–19
Co	7–8.5
Mo	4.6–5.2
Ti	0.3–0.5
Al	0.05–0.15
Nb	-
C	<0.03
Si	<0.1
Mn	<0.1
B (Adding amount)	0.003

When the CVT is in service, the micro-vibration causes a tight-fitting structure of the metal strip steel ring, further resulting in fretting wear. The fretting frequency will affect the change in surface roughness between the friction pairs of the steel ring. When assessing the influence of surface roughness on wear depth, the effect of fretting frequency on surface roughness must first be determined. Here, the influence of fretting frequency on surface roughness is observed using an electron microscope for the scanning test. In particular, a HITACHI Regulus 8100 cold field emission scanning electron microscope is used in this study. This electron microscope can retain the advantages of the SU8100's easy maintenance and easy operation while further improving the test performance. The picture shows the physical picture of the instrument.

Fig. 8. Physical image of HITACHI Regulus8100 cold field emission scanning electron microscope

By using a vibration test bench, the fretting frequencies are gradually set to 30, 60, 90, and 120 Hz, and then the steel ring samples are tested in 3000 cycles. Electron microscopes can be used to select the images with good surface results. As shown in Fig. 9, with the increase in fretting frequency, the surface roughness of the friction pair also increases. Fretting frequency not only increases the amount of wear but also accelerates the mechanical fragmentation of the friction surface, promotes the removal of surface debris, and reduces the protection effect of wear debris. When the fretting frequency is adjusted from 30 to 90 Hz, the roughness and the amount of wear are both increased. However, beyond 90 Hz, the surface roughness and amount of wear both decrease.

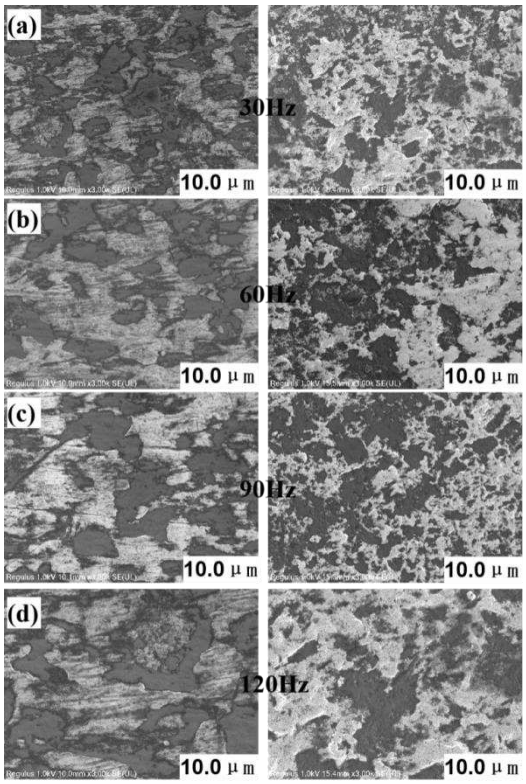

Fig. 9. Surface roughness observation diagram at different frequencies

This trend can be explained by excessive frequency, which can

greatly affect the crack growth rate on the surface of the steel ring. The crack initiation depth is shallow, and its generation rate is slow, resulting in a reduction in the delamination efficiency between the friction pairs. The surface roughness increases with the increase and decrease in frequency.

With the change in the fretting frequency, the wear depth between the friction pairs of the steel ring also undergoes a significant change. Fig. 10 shows the changes in surface wear depth of the steel ring friction pair on the outer side of the first layer, the inner part of the first layer, and the outer steel ring of the second layer with respect to fretting frequency. The wear depth generally increases and then decreases along the axial direction. This trend can be attributed to the increase in fretting frequency. The increase in the amount of wear accelerates the mechanical crushing rate of the friction surface. The faster removal rate of the surface debris, the more apparent the wear depth increases. When the frequency exceeds 90 Hz, the delamination efficiency between the friction pairs decreases; then, the wear depth decreases as the frequency further increases. As shown in Fig. 10(a), when the frequency is adjusted from 30 to 90 Hz, the maximum wear depth of the steel ring friction pair increases from 0.72 to 1.44 μm. As for the at the loose edge, when the frequency increases from 30 to 90 Hz, the maximum wear depth of the steel ring friction pair increases from 0.78 to 1.18 μm. As shown in Fig. 10(c), when the frequency is varied from 30, 60, 90, and 120 Hz, the wear depth at $X/L=0.80$, $X/L=0.72$, $X/L=0.52$, and $X/L=0.56$ also increases rapidly. At the interface, when the frequency is varied from 30 to 90 Hz, the maximum wear depth of the steel ring friction pair increases from 1.24 to 1.73 μm.

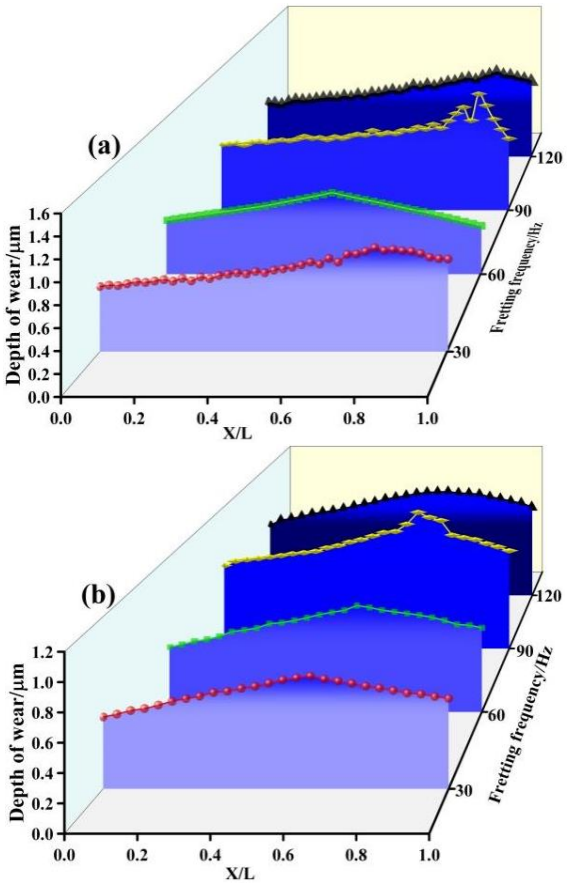

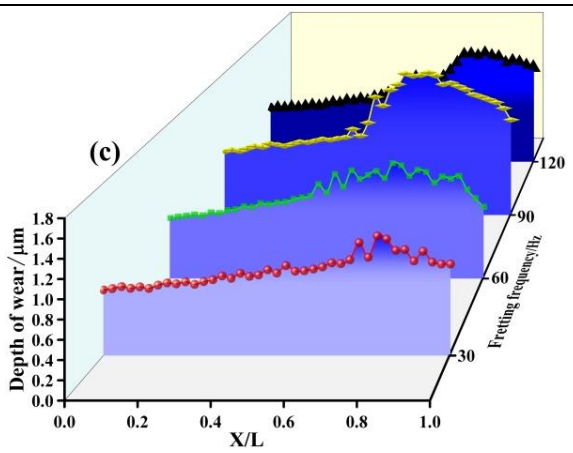

Fig. 10. Wear depths at different positions of the steel ring under varying fretting frequencies: (a) outer side of the first-layer steel ring friction pair; (b) first-layer steel ring friction pair; and (c) second-layer steel ring friction pair.

3.5 Lubrication characteristics

On the basis of the above modeling of the lubrication between the first- and second-layer steel rings, the lubrication characteristics between the two friction pairs are analyzed. The commonly used solution method for point-contact hybrid lubrication is the Newton–Raphson algorithm. This method entails a faster convergence speed and more accurate calculation results. However, this solution process needs to decompose the Jacobian matrix of the equation for one-dimensional linear analysis, rendering the calculation process to be more complicated. Therefore, this simulation process using the Newton iterative algorithm is the best choice.

The array ROU space is initially provided in the calculation process. Moreover, the number of arrays is consistent with the number of nodes. The rough conditions are calculated in advance under the program directory and saved in the corresponding subroutine as a means of facilitating the calculation process. The roughness function is added to the film thickness equation to calculate the change in oil film thickness under the influence of roughness. Finally, as the random roughness is asymmetrical, the Y-direction calculation process is fully executed during the calculation process, and no symmetry processing is performed.

This study attempts to solve the dimensional results of the distribution of film thickness, pressure, and temperature rise between the steel ring friction pairs under the transmission conditions of input torque of $T_p=150N\cdot m$, driving wheel speed of $n_p=5500r/min$, slip rate of $\varepsilon=3\%$, and speed ratio of $i=1$, as shown in the figure. X is the movement direction of the friction plate, while Y is the dimensionless coordinate in the normal direction of the steel ring. Fig. 12 shows the results of the lubrication characteristics between the two friction pairs.

Fig. 11 shows the three-dimensional surface roughness generated on the basis of the built model. The roughness peak of the generated surface does not exceed 1.0, and the roughness peak distribution is random.

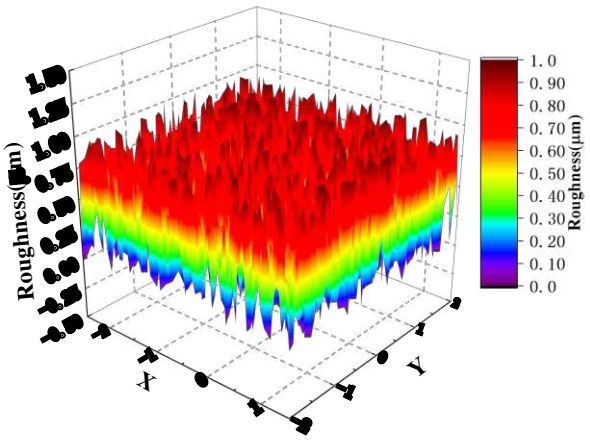

Fig. 11. Three-dimensional roughness surface

Under the influence of random rough peaks, the oil film distribution between the friction pairs is also random. A sharper rough peak implies that a pressure peak will be generated at this time. As shown in Fig. 12(a), the peak pressure at a certain period can reach 1.77 GPa. With the increase in torque and speed, the pressure also increases sharply, and the surrounding lubrication changes into a mixed lubrication, suggesting a danger of oil film rupture.

Fig. 12(b) shows the changes in oil film thickness between the steel ring friction pairs. Oil film thickness can be attributed to the influence of surface roughness. As the wear between the friction pairs gradually increases, the lubricating oil penetrates between the two surfaces of the steel ring. At this time, a comprehensive performance of various lubricating film composition characteristics can be observed between the two friction pairs, and the oil film pressure manifests a rapid change, as depicted by the rough peak. With an ascending trend, the oil film is ultimately elastically deformed due to the pressure exerted by the friction pair on both sides of the oil film, and the first pressure extreme of the oil film appears. At this time, the film thickness also decreases rapidly, i.e., the oil film thickness is 0.3 μm. When the lubricating oil passes through the rough peak, the oil film pressure drops. When the lubricating oil reaches the adjacent rough peak, a necking phenomenon develops, and the oil film pressure again attains an extreme value. At this time, the oil film thickness also reaches an extreme value, i.e., the film thickness is 0.37 μm.

Fig.12(c) presents a graph of the change in oil film temperature under the influence of surface roughness. The temperature change is similar to the pressure change, and the oil film temperature increases sharply at the sharper roughness peak. At the macroscopic level, the frictional force at the peak causes the mechanical energy to be converted into thermal energy, thus increasing the temperature. At the microscopic level, the increase in shear strain of the oil film with respect to the rough peak causes the shear force to further increase, and the oil film gains more shear work, thus causing the temperature to increase. Under the influence of different factors, such as torque, speed, and fretting frequency, the rise in temperature of the oil film with respect to the rough peak can reach approximately 48 °C.

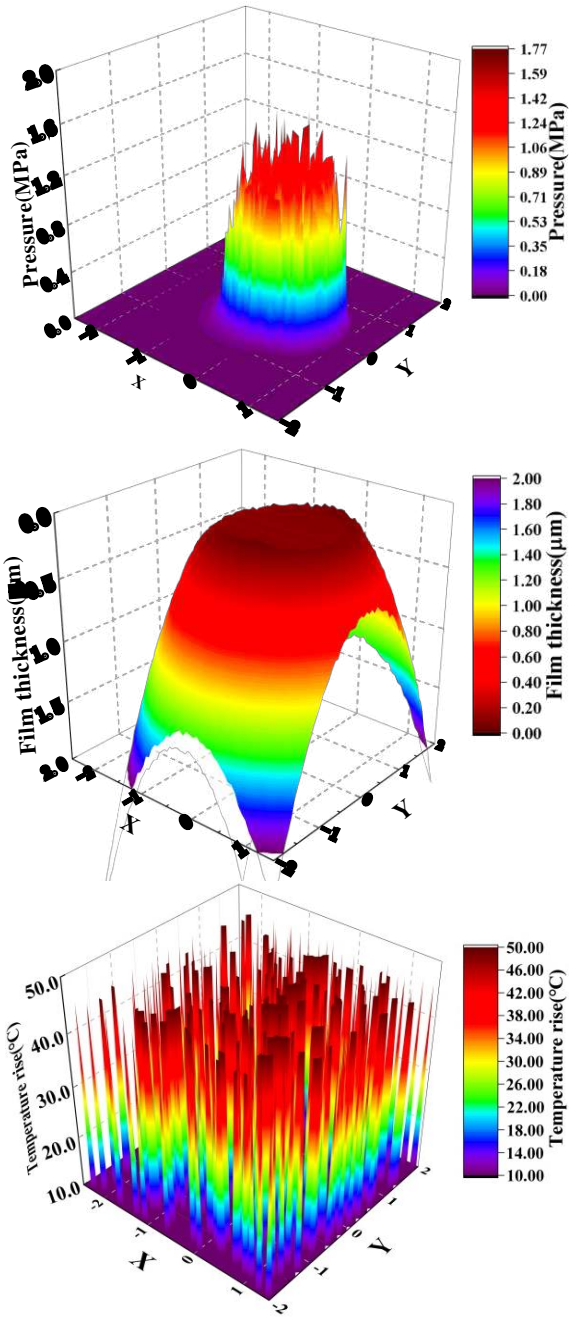

Fig. 12. Simulation diagram of CVT oil film characteristics: (a) pressure change graph; (b) thickness change graph; and (c) temperature rise graph.

4 Safety margin solution

When the CVT is in service, the random roughness and random oil film distribution between the steel ring friction pairs changes under the influence of different factors, such as torque, speed, and fretting frequency. The lubrication state between the friction pairs gradually shifts to mixed lubrication. The overall characteristics of the mixed lubrication represent the comprehensive performance of the composition characteristics of the various lubricating films, the proportion of the lubricating film on the contact surface of the friction pair, and the friction interface morphology and working conditions. During the friction process, the thickness, proportion, and distribution of the lubricating film are constantly changing. When the roughness peak height is greater than the thickness of the maximum lubricating film, a dry friction state is formed at this time,

resulting in surface damage. As the load fluctuates, the mating surface produces fretting slippage and wear. The contact characteristics and relative movement between the belt and pulley are also changed through the transmission of the friction plate. This phenomenon causes the metal belt to slip, the pulley to deflect, and the bearing to creep. In view of ensuring the reliability of the transmission and prolonging the CVT's service life, the expression of the safety margin is obtained according to the previous research content as follows:

$$S = \frac{h(x)}{h_1} - 1 = \frac{\Delta K \sum_{i=1}^{K/\Delta K} \sum_{j=1}^{K_{int}} \upsilon_s \tau_{i,j}(x) ds_{i,j}(x)}{h_0 + \frac{x^2}{2R_x} + \frac{y^2}{2R_y} + h(x,y) + r(x,y)} - 1 \quad (26)$$

When the wear depth is greater than the thickness of the oil film, the safety margin is greater than 0, the wear of the steel ring is aggravated, and the probability of failure and life reduction is increased; thus, the performance is poor at this time. Otherwise, the CVT is in a good safety state. The RD150 CVT is selected as the research object to solve the safety margin. Table 2 shows the structure and working parameters of the selected CVT.

Table 2 Structure and working parameters of CVT

Parameter	Value
Steel ring thickness (mm)	0.18
Modulus of elasticity of metal Steel Ring ($E_2(GPa)$)	192
Poisson's ratio of metal steel ring (υ_2)	0.30
Modulus of elasticity of metal Sheet $E_1(GPa)$	208
Poisson's ratio (υ_1)	0.31
Input torque ($T_p(N \bullet m)$)	30–150
Slip rate ($\varepsilon(\%)$)	1–3
Driving wheel speed ($n_p(r / \min)$)	750–5500
Speed ratio (i)	0.5–2.5
Output torque ($T_p(N \bullet m)$)	25–375

First, the minimum value of the CVT working parameter range is set to the initial value, the step length of the driving wheel speed is set as 100 r/min, the step length of the slip rate is set as 0.1%, the step length of the speed ratio is set as 0.2, and the step length of the torque is set as 10N •M. Then, the temperature change is integrated into the metal belt transmission process, and the safety margin of each operating point is calculated and interpolated. Finally, the corresponding safety margin surface diagram under the aforementioned working conditions is obtained.

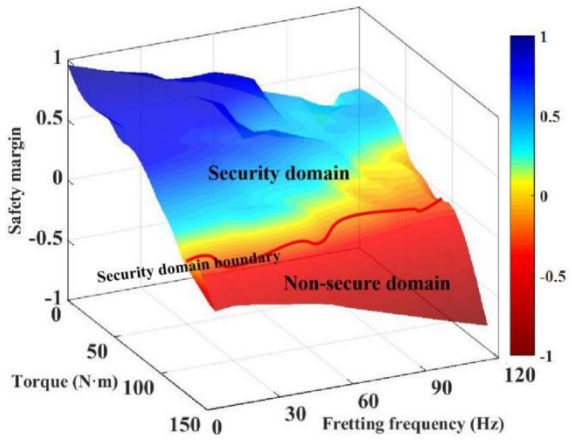

Fig. 13. Friction-pair safe working area of the CVT steel ring

The red area at the bottom right of Fig. 13 indicates that the steel ring friction pair is in the non-safe range. At this time, the efficiency of CVT operation and the safety performance of the CVT is reduced. With the increase in input torque and fretting frequency, the mold back of the lubricating oil film decreases, and the wear depth increases, resulting in a decrease in the overall safety of the steel ring. When the transmitted torque is less than 130N•m, the safety margin exceeds the boundary of the safety zone, suggesting that its relative efficiency and safety performance are reliable, and it can maintain a high output performance. When the transmitted torque is in a non-safe area, a lubricant film is produced. Here, similar to the solid–plastic flow, a significant relative sliding is observed for the surface of the friction pair of the steel ring, and the probability of failure of the friction pair is increased. At this time, the relative sliding speed is reduced; moreover, the safety margin of the lubricating oil film is increased to a safe area, and the oil film is in a safe state during the transmission process.

5 Conclusion

This research focuses on the application efficiency and safety issues of CVT. On the basis of the dissipative wear model that conforms with the steel ring friction pair, a wear depth model related to the wear depth and its influencing variables are established. At the same time, a lubrication model that is consistent with the steel ring friction pair is built. On the basis of the built model, the simulation experiment is implemented under specific working conditions, and the corresponding wear depth and oil film characteristic results are obtained. Finally, the application efficiency and safety issues besides the macro-parameters and micro-lubrication are analyzed deeply. The main conclusions can be summarized as follows:

1) The wear depth of the steel ring friction pair gradually increases with the increase in torque and speed. Along the axial direction, the wear depth increases rapidly at approximately $X / L = 0.8$ and reaches the maximum at $X / L = 1.0$. The wear depth changes with the fretting frequency along the axial direction as a whole to first increase and then decrease. The increase in fretting frequency can be explained by the increase in amount of wear, which leads to the increase in mechanical breakage rate of the friction surface. Subsequently, the removal rate of the surface debris is accelerated. When the frequency exceeds 90 Hz, the delamination efficiency between the friction pairs decreases, and the wear depth decreases as the frequency increases.

2) When the CVT is in service, the heat generated by the friction of the metal belt dissipates through heat conduction. The inner surface of the friction plate is in contact with the side of the steel

ring, and relative sliding shall occur. Thus, the friction work causes a significant increase in the temperature of the contact part. In addition, the saddle surface and contact surface of the steel ring have a lubricating oil in between them, which causes the middle of the steel ring to cool rapidly. The temperature is obviously transferred to the edge of the steel ring. The oil film temperature is randomly distributed and appears in the shape of a peak due to the influence of the rough peak. In addition, a higher temperature peak is generated at the surface rough peak, and the maximum temperature reaches 48 °C.

3) Under the influence of random rough peaks, the oil film distribution between the friction pairs is also random. A sharper rough peak indicates that a pressure peak is generated at this time, and the pressure peak generated during the period can reach 1.77 GPa. Under the influence of the rough peak, the pressure of the oil film as depicted by the rough peak rises rapidly, and the oil film is elastically deformed due to the pressure exerted by the friction pair on both sides of the oil film. The film thickness appears to decrease initially, and the film thickness is 0.3 μm. When the lubricating oil reaches the adjacent rough peak, a necking effect occurs. The oil film thickness decreases sharply, and the film thickness is 0.37 μm.

4) With the increase in torque and speed, the micro-vibration frequency increases gradually. Under the comprehensive consideration of application efficiency and safety, the safety margin decreases gradually with the decrease in macro-parameters. When the transmission torque is greater than 130N• m and when the safety margin drops below 0, the safety margin is in the non-safe area at this time, the transmission efficiency is low, and the probability of safety failure is significantly increased.

6 DECLARATION

Acknowledgements

The authors sincerely thanks to Professor ** of ** University for his critical discussion and reading during manuscript preparation.

Funding

Supported by National Natural Science Foundation of China (Grant No. 51905044)

Availability of data and materials

The datasets supporting the conclusions of this article are included within the article.

Authors' contributions

The author' contributions are as follows: ** was in charge of the whole trial; ** wrote the manuscript; ** assisted with sampling and laboratory analyses.

Competing interests

The authors declare no competing financial interests.

Consent for publication

Not applicable

Ethics approval and consent to participate

Not applicable

References

[1] Mantriota Giacomo and Reina Giulio and Ugenti Angelo. Performance Evaluation of a Compound Power-Split CVT for Hybrid Powertrains. *Applied Sciences*, 2021, 11 (18): 8749-8749.

[2] DONG Jian，DONG Zuomin，CRAWFORD C，et al. Review of continuously variable transmission powertrain system for hybrid electric vehicles [C]//*Proceedings of the ASME 2011 International Mechanical Engineering Congress & Exposition，November 11–17，Denver： ASME*，2011，9：209-219.

[3] Chung C T， Wu C H， Hung Y H . A design methodology for selecting energy-efficient compound split e-CVT hybrid systems with planetary gearsets based on electric circulation . *Energy*, 2021, 230(9):120732.

[4] Ando Taiki et al. Improvement of Transmission Efficiency in CVT Shifting Mechanism Using Metal Pushing V-Belt. *SAE International Journal of Engines*, 2015, 8(3) : 1391-1397.

[5] Zhen-Bing Cai et al. Impact Fretting Wear Behavior of Alloy 690 Tubes in Dry and Deionized Water Conditions[J]. Chinese Journal of Mechanical Engineering, 2017, 30(4) : 819-828.

[6] Fujii T， Kurokawa T， Kanehara S . A Study of a Metal Pushing V-Belt Type CVT-Part 2: Compression Force Between Metal Blocks and Ring Tension[C]// *International Congress & Exposition.* 1993.

[7] Yu-Long Lei et al. Car Fuel Economy Simulation Forecast Method Based on CVT Efficiencies Measured from Bench Test[J]. Chinese Journal of Mechanical Engineering, 2018, 31(1) : 1-16.

[8] S Akehurst et al. Modelling of loss mechanisms in a pushing metal V-belt continuously variable transmission. Part 1: Torque losses due to band friction. Proc*eedings of the Institution of Mechanical Engineers, Part D: Journal of Automobile Engineering,* 2004, 218(11) : 1269-1281.

[9] K Narita and M Priest. Metal-metal friction characteristics and the transmission efficiency of a metal V-belt-type continuously variable transmission. *Proceedings of the Institution of Mechanical Engineers, Part J: Journal of Engineering Tribology*, 2007, 221(1) : 11-26.

[10] S Akehurst et al. Modelling of loss mechanisms in a pushing metal V-belt continuously variable transmission. Part 3: Belt slip losses . *Proceedings of the Institution of Mechanical Engineers, Part D: Journal of Automobile Engineering,* 2004, 218(11) : 1295-1306.

[11]Kevin Lontin and Muhammad Khan. Interdependence of friction, wear, and noise: A review. *Friction,* 2021, : 1-27.

[12] Zhang Yusheng et al. Effect of the frequency on fretting corrosion behavior between Alloy 690TT tube and 405 stainless steel plate in high temperature pressurized water . *Tribology International*, 2021, 164.

[13]Long Xin et al. Effects of dissolved oxygen on partial slip fretting corrosion of Alloy 690TT in high temperature pure water . *Journal of Nuclear Materials*, 2020, 542.

[14] Blades Luke et al. An exploration of debris types and their influence on wear rates in fretting. *Wear*, 2020, 450-451:203252-.

[15] P. Arnaud and S. Fouvry. A dynamical FEA fretting wear modeling taking into account the evolution of debris layer. *Wear*, 2018, 412-413 : 92-108.

[16] Kirk A.M. et al. Interaction of displacement amplitude and frequency effects in fretting wear of a high strength steel: Impact on debris bed formation and subsurface damage. *Wear,* 2021, 482-483.

[17] A.M. Kirk et al. The effect of frequency on both the debris and the development of the tribologically transformed structure during fretting wear of a high strength steel . *Wear*, 2019, 426-427(Pt A) : 694-703.

[18] L. Xin et al. The role of frequency on fretting corrosion of Alloy 690TT against 304 stainless steel in high temperature high pressure

water. *Materials Characterization*, 2017, 134 : 260-273.

[19] Long Xin et al. The Evolution of Fretting Wear Behavior and Damage Mechanism in Alloy 690TT with Cycle Number. *Materials*, 2020, 13(10) .

[20] Ariane Viat et al. Brittle to ductile transition of tribomaterial in relation to wear response at high temperatures. *Wear*, 2017, 392-393: 60-68.

[21] Arman Ahmadi and Farshid Sadeghi and Steve Shaffer. In-situ friction and fretting wear measurements of Inconel 617 at elevated temperatures. *Wear,* 2018, 410-411 : 110-118.

[22] Xin-long Liu et al. Effect of elevated temperature on fretting wear under electric contact. *Wear*, 2017, 376-377: 643-655.

[23]Srivastava N , Haque I . A review on belt and chain continuously variable transmissions (CVT): Dynamics and control. *Mechanism & Machine Theory*, 2009, 44(1):19-41.

[24] Fu Bing,Zhou Yunshan,Hu Kiaolan,Li Hangyang,Liu Yunfeng,Zhang Feitie.Metal belt type continuously variable transmission steel ring friction loss.*Chinese Journal of Mechanical Engineering*,2018,54(14):169-178.

[25] Armando Félix Quiñonez and Guillermo E Morales Espejel. Theoretical analysis of a rolling-sliding elastohydrodynamic lubrication line contact with a subsurface inclusion. *Proceedings of the Institution of Mechanical Engineers, Part J: Journal of Engineering Tribology*, 2019, 233(8) : 1197-1207.

[26] Changjiang Zhou and Zeliang Xiao. Stiffness and damping models for the oil film in line contact elastohydrodynamic lubrication and applications in the gear drive. *Applied Mathematical Modelling*, 2018, 61: 634-649.

[27]Xiangbo Zhang et al. Investigation into gas lubrication performance of porous gas bearing considering velocity slip boundary condition. *Friction*, 2021, : 1-20.

[28] Wang Zongzheng et al. Dynamic contact stiffness of transient mixed lubrication induced by periodic load and speed . *Tribology International*, 2021(1):107225.

[29] Wang Zongzheng et al. Nonlinear Dynamical Behaviors of Spiral Bevel Gears in Transient Mixed Lubrication. *Tribology International,* 2021(1-2): 107022-.

[30] Wang Hongbing et al. Wear life prediction method of crowned double helical gear drive in point contact mixed elastohydrodynamic lubrication. *Wear*, 2021, 484-485.

[31] Zhou Guangwu et al. Analysis of transient mixed elastohydrodynamic lubrication in planetary roller screw mechanism. *Tribology International*, 2021: 107158-.

[32] Wang Zongzheng et al. Nonlinear Dynamical Behaviors of Spiral Bevel Gears in Transient Mixed Lubrication. *Tribology International*, 2021, : 107022-.

[33] Zongzheng Wang et al. Contact stiffness and damping of spiral bevel gears under transient mixed lubrication conditions. *Friction*, 2021, : 1-15.

[34] Chunxing GU, Xianghui MENG, Di ZHANG. Analysis of the coated and textured ring/liner conjunction based on a thermal mixed lubrication model . *Friction*,2018,6 (04):420-431.

[35] Zhuming BI, Donald W. MUELLER, Chris W.J. ZHANG. State of the art of friction modelling at interfaces subjected to elastohydrodynamic lubrication (EHL) . *Friction*,2021,9 (02):207-227.

[36]ARCHARD J F.Contact and rubbing of flat surfaces.*Journal of Applied Physics*,1953,24(8):981-988.

[37]Xiao Yang et al. Experimental and modelling study of interaction between friction and galling under contact load change conditions. *Friction*, 2021, : 1-19.

[38] Florian K. NIG, Christopher SOUS, Georg JACOBS. Numerical prediction of the frictional losses in sliding bearings during start–stop operation . *Friction*,2021,9 (03):583-597.

[39] E Sauger et al. Tribologically transformed structure in fretting . *Wear*, 2000, 245(1) : 39-52.

[40] Yin Zhaoming,Fan Zhimin,Wang Mingkai. Thermal elastohydrodynamic lubrication characteristics of double involute gears at the graded position of tooth waist . *Tribology International*,2020,144(C).